# Laser light scattering by shock waves

J. Panda[a)]
*The University of Toledo, Toledo, Ohio 43606*

G. Adamovsky
*NASA Lewis Research Center, Cleveland, Ohio 44135*

NASA-TM-111739

Scattering of coherent light as it propagates parallel to a shock wave, formed in front of a bluff cylindrical body placed in a supersonic stream, is studied experimentally and numerically. Two incident optical fields are considered. First, a large diameter collimated beam is allowed to pass through the shock containing flow. The light intensity distribution in the resultant shadowgraph image, measured by a low light CCD camera, shows well-defined fringes upstream and downstream of the shadow cast by the shock. In the second situation, a narrow laser beam is brought to a grazing incidence on the shock and the scattered light, which appears as a diverging sheet from the point of interaction, is visualized and measured on a screen placed normal to the laser path. Experiments are conducted on shocks formed at various free-stream Mach numbers, $M$, and total pressures, $P_0$. It is found that the widths of the shock shadows in a shadowgraph image become independent of $M$ and $P_0$ when plotted against the jump in the refractive index, $\Delta n$, created across the shock. The total scattered light measured from the narrow laser beam and shock interaction also follows the same trend. In the numerical part of the study, the shock is assumed to be a "phase object," which introduces phase difference between the upstream and downstream propagating parts of the light disturbances. For a given shape and $\Delta n$ of the bow shock the phase and amplitude modulations are first calculated by ray tracing. The wave front is then propagated to the screen using the Fresnel diffraction equation. The calculated intensity distribution, for both of the incident optical fields, shows good agreement with the experimental data. © *1995 American Institute of Physics.*

## I. INTRODUCTION

A significant change of gas density across a shock is accompanied by a change in the refractive index. Upstream of the shock is a region of lower refractive index and downstream is a region of higher refractive index. A large deflection of light rays across this change in refractive index makes the shock easily visible in schlieren and shadowgraph images. The phenomenon is usually explained with the laws of geometrical optics (Merzkirch,[1] p. 115). However, a shock is also expected to cause light diffraction, as the extremely small thickness effectively makes it a sharp interface between the optically different upstream and downstream regions. The objective of the present work is to explore the light diffraction effects caused by a shock wave. This paper presents extensive experimental evidence and a numerical calculation based on the Huygens–Fresnel principle[2] to explain this phenomenon.

Two different optical conditions, both of which involve significant diffraction effects as laser light propagates parallel to a shock surface, are considered. The first one is the well-known shadowgraph situation, where a large diameter collimated laser beam is allowed to pass through the shock containing region and the shadowgraph image formed on a screen is studied.

The second is somewhat unknown and was first reported by Panda.[3,4] It involves a narrow laser beam brought to a

grazing incidence on a shock surface. In this situation a thin diverging light sheet is found to appear from the point of interaction. The visible divergence angle of the light sheet is very large, up to $\pm 10°$ depending upon the shock strength, and the light appears both upstream and downstream of the shock. When a screen is placed normal to the laser path, the cross-section of the sheet appears as a long, bright streak. The scattered light is found to disappear at all other incidence angles when the laser beam pierces the shock. The optical phenomenon is also believed to appear primarily due to diffraction of laser light by shock waves; however, sufficient evidence to determine the exact nature of the phenomenon was absent. It has been demonstrated that the phenomenon can be used as the basis of a novel shock detection technique[3,5] which is convenient in detecting unsteady shock motion. A major motivation of this work is to determine the effects of various fluid dynamic and optical parameters on the scattered light, as well as to establish the physics behind the phenomenon.

Evidence of diffraction fringes in the shadow image of a shock can be found in many earlier experiments.[6,7] Pfeifer *et al.*[8] have shown that for a plane shock, the zeroth diffraction order is a minimum, which appears in the shadowgraph to form the dark band. Merzkirch[1] also discusses that, when the incident light waves propagate parallel to the surface of the shock the major contribution to the formation of a shadow is light diffraction (see discussion on p. 133). However, all of these discussions are very limited in scope and frequently the diffraction effects are overlooked. Wide angle scattering of a narrow beam of light by conducting cylinders has been reported earlier in the literature (see Langois

[a)]Resident Research Associate, NASA Lewis Research Center, Cleveland, Ohio 44135. Corresponding author; tel.: 216-433-8891; fax: 216-433-5802; e-mail: panda@yaz.lerc.nasa.gov

*et al.*[9]). However, the present problem involving shock waves is very different. Optical properties of the scattered light such as the intensity distribution, fringe spacing, and the effects of various fluid dynamic parameters were not studied for the diffraction effects caused by a shock wave.

In the experimental part of this study a steady bow shock, formed ahead of a bluff cylinder placed in a supersonic free stream, is used to study such effects. Light intensity distributions for both the wide angle scattering from a narrow beam and diffraction fringes in shadowgraph images are measured for various free-stream Mach numbers and total pressures. In the numerical part of this study, the phenomena are modeled as due to the phase difference between the light waves traveling upstream and downstream of the shock. The two-dimensional (2-D) analysis assumes that the incidence disturbance field is made of plane and parallel waves to model the shadowgraph image and a Gaussian strip to model the narrow laser beam and shock wave interaction. The diffraction patterns are calculated and presented after describing the experimental results. Finally, the similarities and differences between the two situations and various other parameters that may affect the diffraction phenomena are discussed in the conclusion.

## II. EXPERIMENTAL FACILITY

The experiments were conducted in a continuous, 127 mm×127 mm supersonic wind tunnel at the NASA Lewis Research Center. Details of the tunnel can be found elsewhere.[10] In brief, the tunnel is supplied by compressed air which is discharged into a low vacuum altitude exhaust system. The free-stream Mach number can be varied from 1.5 to 3.0 by changing the nozzle contour. The free-stream total pressure, $P_0$, also can be varied independently from 134 to 375 KPa. The total temperature of the supplied air is the same as that of the ambient air (294 °K). For the present experiment the test section was equipped with two scratch free plexiglass windows, each 25.4 mm thick. The cylindrical bluff body used to produce a bow shock was mounted edge on with its axis along the flow direction. It was 12.7 mm in diameter and was mounted on a sting at the center of the tunnel.

The experiments were conducted at three different free-stream Mach numbers: 1.5, 2.0, and 2.5, and five different free-stream total pressures: 375, 306, 237, 168, and 134 KPa. For the highest Mach number of 2.5 the tunnel could not be started at the lowest total pressure of 134 KPa, and for the lowest Mach number of 1.5 operations were limited to a maximum $P_0$ of 237 KPa by the maximum allowable mass flux of air supplied to the tunnel.

A 4 mW, random polarization, He–Ne Laser (632.8 nm wavelength) was used as the light source for all experiments. A polarizer, placed in front of the laser was used to change incident beam polarization, and a combination of the polarizer and a neutral density filter was used to cut down the laser power when needed.

The scattered light patterns were visualized on a semi-transparent screen (similar to a ground glass) placed normal to the laser path. The images on the screen were photographed using a cooled CCD camera which provided quan-
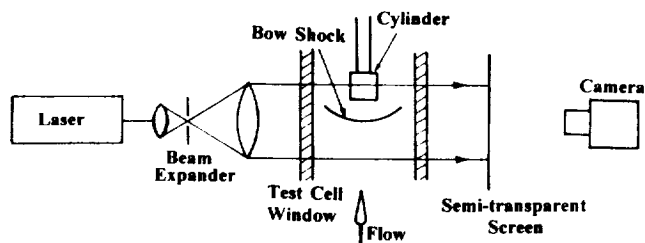


FIG. 1. Schematic of shadowgraph arrangement.

titative information of the light intensity distribution on the screen. The 12-bit, 576×384 pixel camera has a separate refrigeration unit to cool the camera head to −45 °C; thereby dropping the dark current significantly. This low noise feature makes the camera useful for measuring low levels of light. The camera has its own controller which, in turn, is interfaced with a 486DX Personal Computer (PC). Images obtained by the CCD camera were stored in the PC and are post-processed to obtain quantitative information. Various Nikon lenses were used on the camera head to expose a wide range of area on the screen.

A laser shadowgraph system was used to obtain a large diameter collimated beam (Fig. 1). The narrow beam from the He–Ne laser was allowed to pass through a beam expander (made up of a microscope objective, a 25 μm spatial filter and a 300 mm focal length lens) and was allowed to pass through the test section. The shadowgraph image formed on the semitransparent screen placed on the other side of the test section was photographed either by the CCD camera or by a 35 mm camera.

## III. EXPERIMENTAL RESULTS

Figure 2 shows shadowgraph images of the bow shock formed in front of the bluff body for two different free-stream Mach numbers. For all figures presented in this paper, flow is from left to right. The bow shock is found to become more curved and to move closer to the bluff cylinder as the
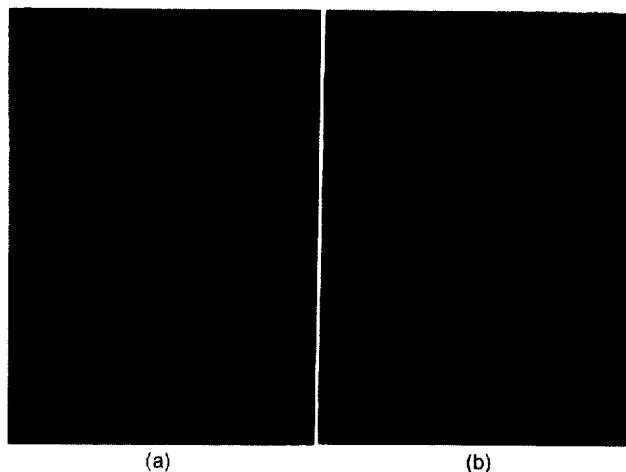


FIG. 2. Shadowgraph image of the bow shock formed ahead of a bluff cylindrical body; (a) $M = 1.5$ and (b) $M = 2.0$. Flow is from left to right.

J. Panda and G. Adamovsky

free-stream Mach number is increased. However, for a fixed $M$, as $P_0$ is changed the shock shape and its location are not affected.

A steady shock is essential to achieve the experimental goal. To check the shock steadiness, video recordings of the shadowgraph images were obtained by a separate light intensified CCD camera that can be gated to a fast shutter speed of 20 ns. A frame by frame analysis showed that the shock was extremely stationary up to $M \le 2.5$, above which it meandered at a very low frequency, perhaps due to the proximity to the bluff body.

## A. Diffraction effects in shadowgraph image of shock

The diffraction effects are not visible in the 35 mm photographs of Fig. 2. To highlight the detail of the shock shadow a small region around the tip of the bow shock along the centerline of the cylindrical body was photographed using the low light CCD camera. Two different images were taken: one without the any airflow, "no-flow" image, and a second one with the flow on. Subsequently, the no-flow image was subtracted from the "flow" image to determine the changes caused by the shock. The processed data clearly show the dark shadow cast by the shock and clear fringes upstream and downstream of the shock. Figures 3(a) and 3(b) show two such processed images of the bow shock in $M = 1.5$ free-stream at two different free-stream total pressures. The screen, from which the shadowgraph images were photographed, was placed 685 mm away from the shock location. The dark band representing the shadow of the shock appears very thick due to a magnification of ~8 from Fig. 2.

A special problem encountered with the laser shadowgraph system is the speckle noise produced by small dust particles on the wind tunnel windows. This random optical noise is easily visible in Figs. 3(a) and 3(b). To cancel out the background noise the light intensity data was averaged over a transverse band of 30 pixels. The intensity values presented in Fig. 3(c) are also normalized by the average intensity of the no-flow image. The resultant intensity distribution shows that the first fringe downstream of the central dark band is always the brightest. Both downstream and upstream fringes are indicative of light diffraction, whereas some of the extra light in the downstream fringes can also be interpreted from geometrical optics due to refractive bending of light.

It is found that the width of the central dark band and the intensity modulation in the fringes depend on the free-stream total pressure $P_0$ and Mach number $M$. For a fixed $M$, the light patterns become weaker as $P_0$ is decreased. This is clearly visible from the two different $P_0$ cases shown in Fig. 3. It is possible to simplify this dependency by analyzing the fluid dynamic and the optical properties of the shock. Table I presents such properties calculated for the tip region of the bow shock. Since the shock is normal to the flow direction at this location, flow properties downstream of the shock are obtained by applying the normal shock relations. The refractive indices (n) are calculated assuming ideal gas behavior, and by applying the Gladstone–Dale relationship:[1] $n - 1 = C\rho$, where $\rho$ is the local density of air and $C$ is the Gladstone–Dale constant ($C = 2.25 \times 10^{-4}$ m³/Kg used for the laser wavelength). Data in Table I show that as $P_0$ is



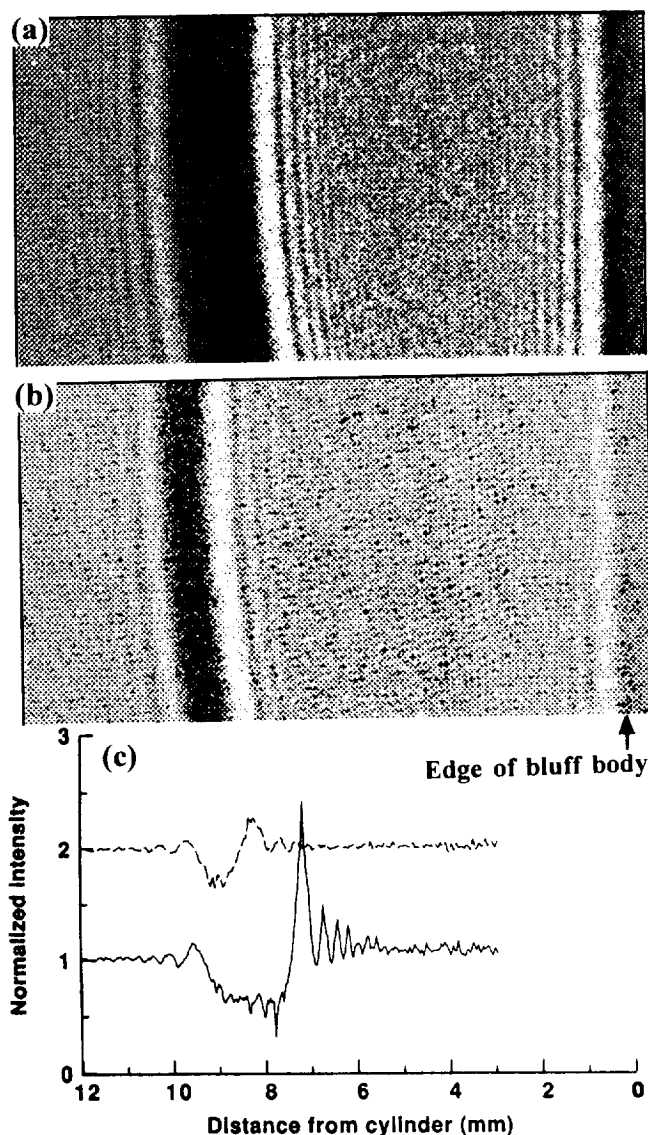FIG. 3. (a) and (b) Enlarged view of the tip region of the bow shock obtained with a CCD camera; $M = 1.5$, $P_0 = 237$, and 134 KPa, respectively. (c) Light intensity distribution along centerline, $-P_0 = 237$ KPa and $---P_0 = 134$ KPa. The latter is shifted by one major division.

decreased keeping $M$ constant, the air density, both upstream and downstream of the shock, decreases. The refractive indices also follow the same trend. The last column of Table I shows that the net difference of the index of refraction, $\Delta n$, between the upstream and downstream regions decreases with a decrease in $P_0$. The dependence on $M$ for a fixed $P_0$, however, is not straightforward as the density change across a shock is a nonlinear function of $M$. Nonetheless, it is found that the jump in the refractive index across a shock is the single most important parameter that controls the shadow formation in the shadowgraph images. This is shown in Fig. 4 where the width of the central dark band, representing the shadow of the shock, is plotted against $\Delta n$. The data points are obtained from shadowgraph images on a screen placed at a fixed distance of 216 mm away from the shock and for different $M$ and $P_0$ conditions. The normalized light intensity distributions, similar to Fig. 3(c), were obtained from

Phys. Fluids, Vol. 7, No. 9, September 1995

J. Panda and G. Adamovsky    2273

TABLE I. Shock properties relevant to the light scattering phenomenon.

| Mach No. $M$ | | Freestream total Pressure $P_0$, KPa | Air density Kg/m$^3$ | | Refractive index | | |
| Upstream | Downstream | | Upstream | Downstream | Up, $n_u$ | Down, $n_d$ | Diff., $\Delta n$ |
| --- | --- | --- | --- | --- | --- | --- | --- |
| | | 237 | 1.115 | 2.076 | 1.000 252 | 1.000 468 | 0.000 217 |
| 1.5 | 0.70 | 168 | 0.791 | 1.473 | 1.000 178 | 1.000 332 | 0.000 154 |
| | | 134 | 0.629 | 1.171 | 1.000 142 | 1.000 264 | 0.000 122 |
| | | 375 | 1.027 | 2.738 | 1.000 232 | 1.000 618 | 0.000 386 |
| | | 306 | 0.838 | 2.235 | 1.000 189 | 1.000 504 | 0.000 315 |
| 2.0 | 0.58 | 237 | 0.649 | 1.732 | 1.000 147 | 1.000 391 | 0.000 244 |
| | | 168 | 0.461 | 1.228 | 1.000 104 | 1.000 277 | 0.000 173 |
| | | 134 | 0.366 | 0.976 | 1.000 083 | 1.000 220 | 0.000 138 |
| | | 375 | 0.588 | 1.959 | 1.000 133 | 1.000 442 | 0.000 309 |
| | | 341 | 0.534 | 1.779 | 1.000 12 | 1.000 401 | 0.000 281 |
| | | 306 | 0.48 | 1.6 | 1.000 108 | 1.000 361 | 0.000 253 |
| 2.5 | 0.51 | 272 | 0.426 | 1.419 | 1.000 096 | 1.000 320 | 0.000 224 |
| | | 237 | 0.372 | 1.239 | 1.000 084 | 1.000 280 | 0.000 196 |
| | | 168 | 0.264 | 0.879 | 1.000 059 | 1.000 198 | 0.000 139 |

each image and the thickness of the shadow is measured as the width between the unit intensity points of the trough representing the shock shadow. The refractive index jump, $\Delta n$, is obtained from Table I. Figure 4 shows that the shadow width increases with $\Delta n$ and is independent of $M$ and $P_0$. The implication of this result is that the only way any change in the fluid dynamic parameters affects the optical scattering is by changing the optical property of the medium, that is the net jump in the refractive index across a shock. Somewhat similar behavior is also observed when a narrow laser beam is used to study the shock laser interaction. This is discussed next.

## B. Narrow laser beam and shock interaction

Figure 5 shows a schematic of the arrangement to measure the scattered light produced from such an interaction. When the narrow laser beam is brought to a grazing incidence on the bow shock, the scattered light appears as a diverging sheet from the main laser beam. For all data pre-
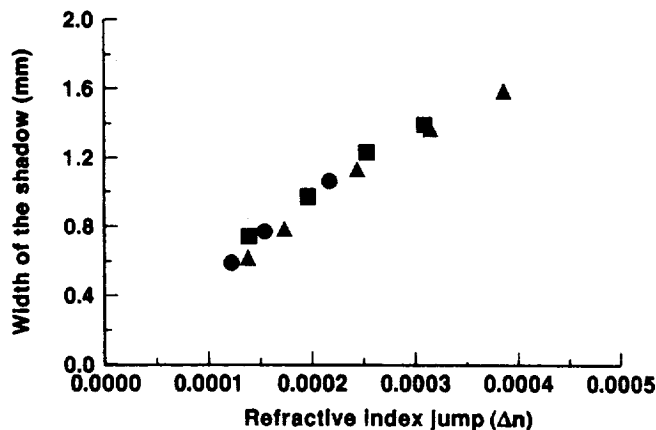
sented in this paper, the laser beam is made to touch the tip region of the bow shock. The light patterns, as photographed from a screen placed normal to the laser path and 480 mm away from the shock, are shown in Fig. 6. The long streaks, extending far upstream and downstream from the shock, are aligned with the flow direction. If the laser beam is moved to touch any other part of the bow shock, the streaks are found to become inclined along the local normal to the shock surface. Various other features including the directional dependence of the scattered light has been discussed earlier.[3,4] The scale at the bottom of the figure shows the angular spread ($\theta$) of the scattered light. The angular spread angle is defined as

$$\theta = \tan^{-1}$$

$$\times \left( \frac{\text{Distance on screen from center of the laser spot}}{\text{shock to screen distance}} \right),$$

(1)

and is also shown in the schematic of Fig. 5. The wide angle light streaks are definite evidence of diffraction effect. Figures 6(b)–6(d) correspond to a decreasing $P_0$ while the freestream Mach number was kept constant. Clearly, the phenomenon weakens progressively as $P_0$ is decreased. Note that the laser beam, whose cross section is seen as a bright central spot, splits into two parts after touching the shock.
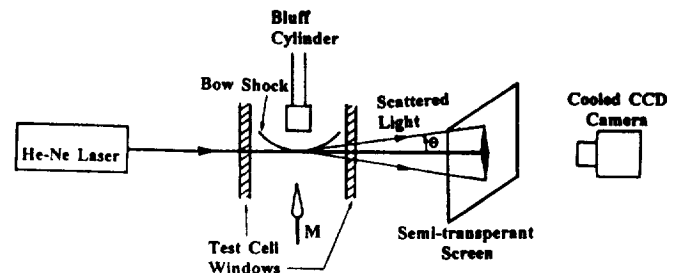


FIG. 4. Width of the central dark band in shadowgraph image of shock versus the refractive index difference created across the shock; ●, $M$=1.5; ▲, $M$=2.0; ■, $M$=2.5.



FIG. 5. Schematic of the arrangement to visualize and measure the wide angle light scattering phenomenon.

2274    Phys. Fluids, Vol. 7, No. 9, September 1995
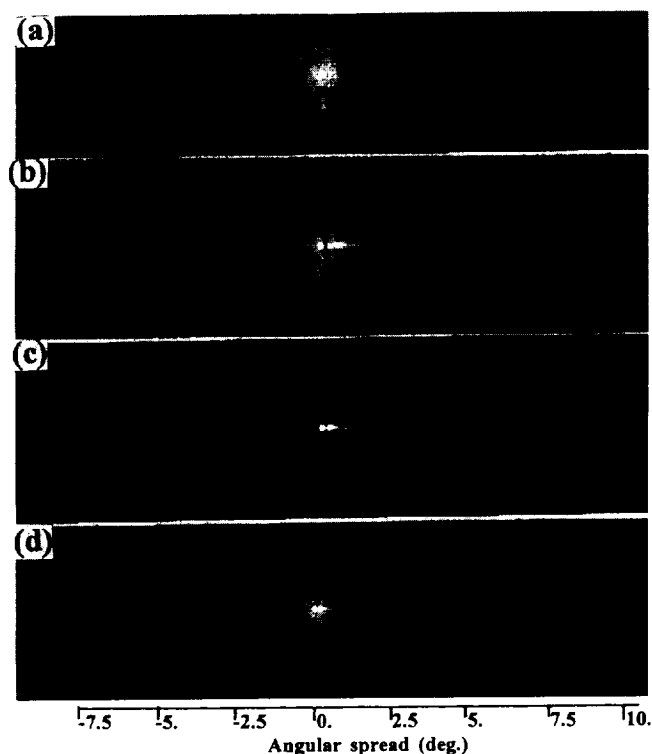
J. Panda and G. Adamovsky

FIG. 6. Cross-sectional views of the laser beam showing the wide angle light scattering; (a) no-flow; (b)-(d) interaction with shocks formed in $M=2.0$ flow and $P_0=306$, 237, and 168 KPa, respectively.

Quantitative measurement of the light intensity distribution in the long streaks was not straightforward, as the intensity varied by many orders of magnitude from the center of the laser beam to the visible end of the streaks. To satisfy the conflicting requirements of avoiding saturation from the intense main laser beam and having sufficient exposure to capture the weak tail, data were obtained in two steps. At first, the laser power is reduced considerably by placing a neutral density filter in the path of the beam, and the paraxial region around the main beam is photographed. The images show only the change in the main laser beam; little information about the scattered light is present. Figures 7(a) and 7(b) show two such photographs of the main laser beam with and without the presence of the scattering phenomenon. The central dark region between the split portions of the beam in Fig. 7(b) corresponds to the shadow formed by the shock. The light intensity distribution measured from the pixels along the image centerline is plotted in Fig. 7(c). The intensity data are normalized by the maximum value in the undisturbed laser beam. Clear splitting of the beam and spreading of light energy primarily in the downstream direction are visible in this figure. A comparison of the scales showing the spread angle in Figs. 6 and 7 shows that the latter corresponds to a small region close to the main beam.

A second set of images was taken to measure the intensity distribution in the wide angle streaks (Fig. 8). For these measurements the incident laser beam had to be brought back to its full intensity and a 12 mm wide beam stop was placed just in front of the semitransparent screen to block the main beam. The latter was necessary to avoid blooming of
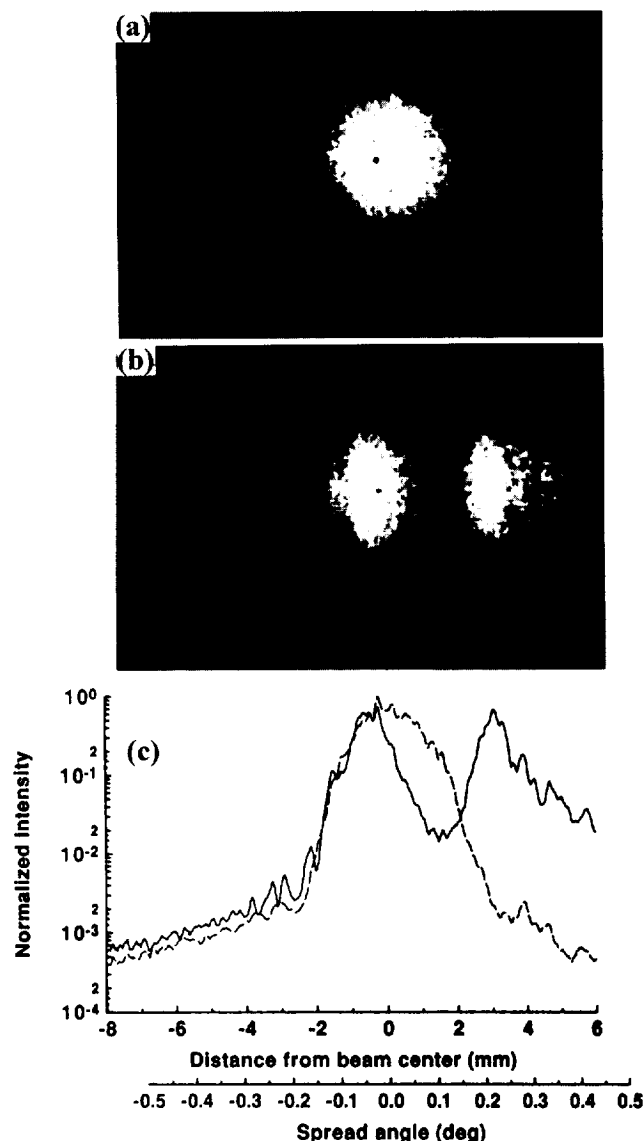
FIG. 7. Enlarged view of the main laser beam; (a) no-flow; (b) interaction with a shock in $M=2$ and $P_0=237$ KPa flow; (c) light intensity distribution along centerline; — — —, no-flow; ——$M=2.0$, $P_0=237$ KPa.

the CCD elements from the intense light of the full power beam. The shadow cast by the beam stop is marked in this figure. The diffraction effects from the beam stop itself are negligible as it is placed just in front of the screen. Once again, a comparison between the abscissa of Figs. 7 and 8 shows that the entire paraxial region covered in the former falls into the shadow of the beam stop.

The intensity distribution in the long light streaks for various upstream total pressure conditions is shown in Fig. 8. The free-stream Mach number is kept constant at 2.0 for all of these measurements. All data are normalized by the maximum intensity value measured in the $M=2.0$, $P_0=375$ KPa condition. The intensity of the scattered light is found to diminish with a drop in the free-stream total pressure, $P_0$. Recall that $P_0$ determines the jump in the refractive index across the shock. The scenario is consistent with the earlier description of shadowgraph images.

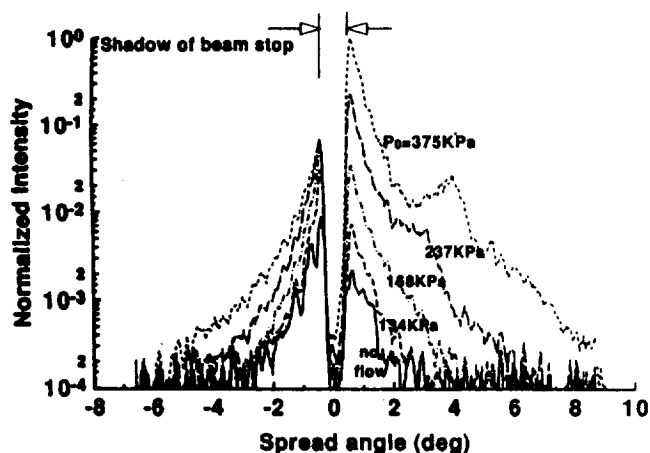For an application of the light scattering phenomenon as

Phys. Fluids, Vol. 7, No. 9, September 1995

J. Panda and G. Adamovsky 2275

FIG. 8. Intensity distribution in the scattered light from interaction with shocks formed in $M=2.0$ flow. Shock to screen distance$=292$ mm.

a detection technique for shock, it is useful to obtain a relationship between the net scattered light and the shock strength. The latter is measured as the jump in the refractive index, $\Delta n$, across a shock. The net scattered light, $I_T$, is expected to be proportional to the area covered under each curve of Fig. 8. A plot of $I_T$ versus $\Delta n$ is shown in Fig. 9. All data were obtained from measurements with a fixed laser power and a fixed shock to screen distance.

The close-to-linear dependence in the semilog plot of Fig. 9 shows that $I_T$ increases almost exponentially with $\Delta n$. Unlike the shadowgraph situation, $I_T$ is also dependent on the free-stream Mach number. However, the calculated values of $I_T$ are not very accurate, as the scattered light from the paraxial region of beam propagation was blocked by the beam stop, and therefore, is excluded from the calculation.

The effect of the polarization of light on the wide-angle scattering phenomenon was studied by placing a polarization rotator on the path of the incident laser beam. However, within the measurement accuracy, the phenomenon is found to be independent of the light polarization.
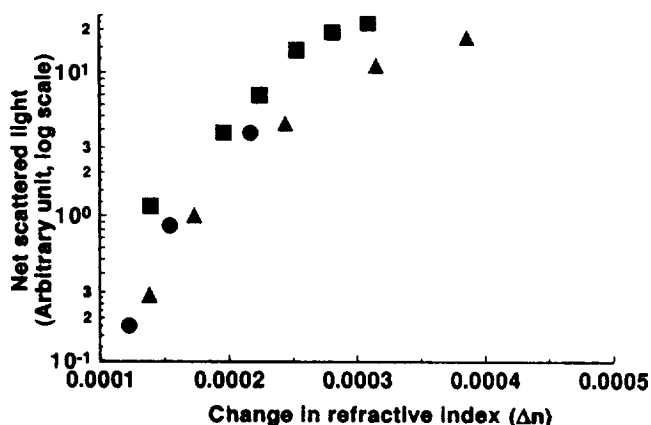


FIG. 9. Net scattered light in narrow laser beam and shock interaction versus the refractive index jump across the shock; ●, $M=1.5$; ▲, $M=2.0$; ■, $M=2.5$.

## IV. ANALYSIS

According to the laws of geometrical optics, light rays are expected to bend only along the gradient of refractive index, which is along the downstream direction for a normal shock. However, clear violations are observed in the presence of the upstream fringes in the shadowgraph image and in the upstream part of the scattered light in narrow laser beam and shock interaction. The deflection angle, $\gamma$, of a laser beam while crossing a shock has been calculated by Kriksunov and Pliev[11] following the paraxial ray equation, $\tan \gamma = \int_0^z (dn/d\xi)dz$, (where $z$ is the beam propagation direction and $\xi$ is the flow direction) and is found to be a fraction of a degree. The visible spread angle of the long streaks, on the other hand, can be as large as $\pm 10°$.

Shock waves are also known to cause light reflection. However, the reflectivity of the shock fronts are very small. Measurements by Hornig[12] showed that the optical reflectivity of a strong shock is in the order of $10^{-6}$, while the present data show that the net scattered light from a narrow laser beam and shock interaction can be greater than 1% of the incident laser power. Therefore, contribution from the reflected light to the net scattered light is expected to be minimal.

The light scattering phenomenon in the two situations considered here are indicative of a strong diffraction effect. Noticeably, both phenomena appear when light disturbances travel parallel to the surface formed by a shock. In this condition, a part of the beam propagates upstream and the rest downstream of the shock. The difference in the optical path length between the two parts of the beam produces phase variation. Therefore, a shock wave can be thought of as a "phase object"[2] that does little change to the magnitude of the incident light disturbance, but considerably distorts the phase. The resulting diffraction pattern can be calculated by an application of the Huygens–Fresnel principle. In an elementary way, Pfeifer et al.[8] used the above principle to calculate the light intensity variation caused by the passage of a normal shock in a shock tunnel. It may be worthwhile to mention that any compressible flow, in general, is a phase configuration due to the variation in the refractive index with little absorption taking place, and a shock wave is the extreme case.

The present analysis is performed for the two incident light disturbance fields for which experiments were performed. At first, the ray tracing method is used to calculate the phase and intensity variation in a bundle of light rays just after crossing the shock wave. Next, scalar diffraction theory is applied to calculate the irradiance distribution after the emerging rays propagate to the screen.[13] Figure 10 shows a schematic of the steps involved. The calculation is performed in 2D and for the tip region of the bow shock. The $\xi$ axis is along the flow direction and the $z$ axis is along the light propagation direction. The shape of the bow shock is obtained from the shadowgraph image. A simple curve fit, $\xi = a[1 - \cos(bz)]$, where $a$ and $b$ are adjustable constants, is found to be sufficient to analytically express the shock profiles. The values of the constants for the $M=1.5$ and 2.0 cases are, respectively, $a=+68.62$ and $+70.5$ mm, and $b=0.0191$ and $0.0232$ mm$^{-1}$. The refractive indices are as-
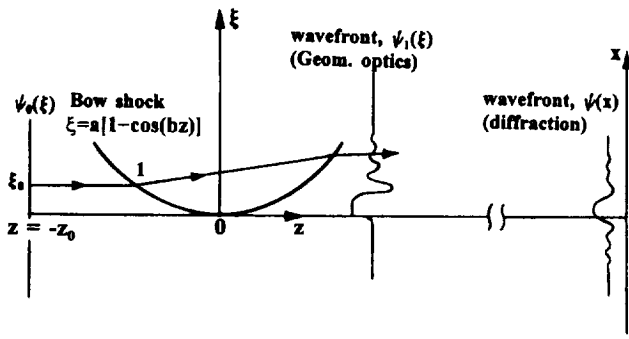
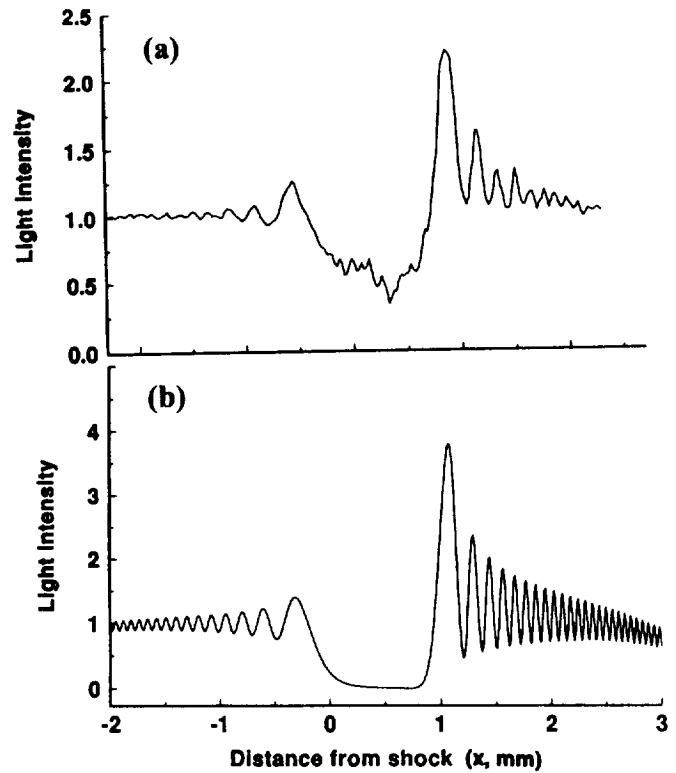FIG. 10. Schematic of the procedure to calculate light scattering by shock.



FIG. 11. A comparison between (a) experimental and (b) calculated intensity distribution in the shadowgraph image of shock; $M = 2.0$, $P_0 = 237$ KPa, shock to screen distance $= 216$ mm.

sumed to be constant, $n_u$, everywhere upstream, and $n_d$, everywhere downstream of the shock.

The ray tracing calculations start with an initial intensity distribution $\psi_0(\xi)$ from the position $z = -z_0$, away from the shock. The deflection of each ray, while crossing the shock front, is determined by an application of Snell's law. For example, at point 1 in Fig. 10, $\sin \delta_u / \sin \delta_d = n_d/n_u$, where $\delta_u$ is the incidence angle and $\delta_d$ is the refracted angle. After each ray emerges from the shock it is traced back to a virtual line of origin, $z = z_v$, to avoid ray crossing and also to obtain a standard reference line to start the diffraction calculation. The point of intersection of the traced back first ray, above $\xi = 0$, to its original path is used to determine $z_v$. The complex wave front at this virtual line of origin is determined as $\psi_1(\xi) = \alpha(\xi)\exp[i\phi(\xi)]$, where phase $\phi(\xi) = kS(\xi)$, where $S(\xi)$ is the computed optical path and $k$ is the wave number $2\pi/\lambda$; $\lambda$ is the wavelength of the laser light. The amplitude $\alpha(\xi)$ is determined using conservation of energy along ray bundles. Assuming the rays do not cross, the energy between 0 to $\xi_0$ at the starting line should be the same as that between 0 to $\xi$ at the virtual line of origin. This provides the integral equation

$$\int_0^{\xi_0} \psi_0 \psi_0^* \, d\xi = \int_0^{\xi} \psi_1 \psi_1^* \, d\xi, \qquad (2)$$

where the superscript * represents the complex conjugate.

In the next step, the calculated wavefront $\psi_1(\xi)$ is propagated to the screen, $z$ distance away from the shock, using the Fresnel diffraction equation,

$$\psi(x) = \frac{K e^{ikz}}{z} \int_{-\infty}^{\infty} \psi_1(\xi) e^{(ik/2z)(x - \xi)^2} d\xi, \qquad (3)$$

where $\psi(x)$ is the optical disturbance on the screen and $K$, the "obliquity factor" $= -i/\lambda$. The complete procedure to numerically calculate the Fresnel integral is provided by Weaver[14] (see Chap. 8) and will not be repeated here. In brief, it involves casting the above equation in a convolution form and applying Fourier transform and an inverse transform. The calculations use Fast Fourier Transform routines from the Numerical Recipes[15] and are performed in the same PC used for data acquisition.

Figure 11(b) shows the calculated light intensity distribution on a screen when the incident light disturbance $\psi_0(\xi)$ is assumed to consist of plane, parallel waves. This situation corresponds to the shadowgraph image of the shock. For a

direct comparison, experimental data obtained from an identical condition is shown in Fig. 11(a). All major features, such as the central shadow and the fringe patterns upstream and downstream of the shock, are clearly captured in the numerical calculations. The width of the shock shadow in the experimental and the numerical data are nearly the same. However, the fringe spacings are slightly different and the peak intensity in the fringes are higher in the calculated data. The latter is due, possibly, to an error in the experimental data, which is contaminated by a high level of speckle noise. Moreover, as mentioned earlier, the experimental data were also averaged over 30 pixels.

Note that the zero on the abscissa of Fig. 11 represents the position of the shock, positive numbers represent downstream and negative numbers represent upstream distance. The numerical data in Fig. 11(b) demonstrate that the shock is located at the upstream edge of the thick shadow. This is consistent with the discussion of Merzkirch.[1]

It is interesting to note an important difference between the present analysis of light scattering by shock and the classical Fresnel diffraction by a straight edge.[2] Both problems are similar in the presence of a sudden discontinuity; however, there is an important difference between the two. The textbook treatment of diffraction by a straight edge assumes an opaque half-screen that completely absorbs the incoming light, while a shock wave does not cause any light absorption. For the latter, transmitted light beyond the "straight edge" created by a shock produces the downstream fringes in the shadowgraph situation, and for the former, light intensity

Phys. Fluids, Vol. 7, No. 9, September 1995
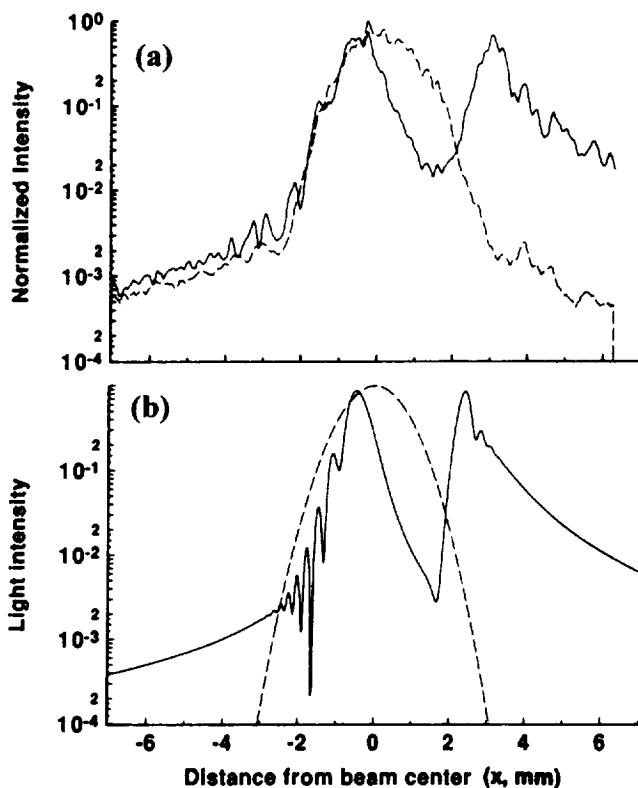
J. Panda and G. Adamovsky     2277

FIG. 12. A comparison between (a) experimental and (b) calculated intensity distribution in the narrow laser beam and shock interaction; $M=2.0$, $P_0=237$ KPa, shock to screen distance$=737$ mm; $---$undisturbed beam; —after interaction with shock.

approaches zero very quickly inside the geometrical shadow of the opaque screen.

To calculate the light scattering from the narrow laser beam and shock interaction, the incident light intensity distribution is changed to that of a 2 mm diameter Gaussian beam with a peak intensity of unity, $\psi_0(\xi)=\exp(-\xi^2/4)$. The beam diameter corresponds to the estimated experimental value at the shock position. Since the calculations are performed in 2D, the incident field is, in effect, a Gaussian strip of light. The calculated diffraction pattern is shown in Fig. 12 along with the experimental data obtained for the same condition. Once again, the primary features: splitting of the beam into two parts, strong scattering in the downstream direction and a weaker scattering in the upstream direction, are well represented. Similar to the shadowgraph situation, the experimental data also suffer from speckle noise which obliterates the weak fringes, predicted by the computational data.

The primary shortcoming of the numerical calculation is the 2-D modeling of a three-dimensional (3-D) situation. The bow shock is axisymmetric; however, the present calculation assumes that the shock shape remains constant in the missing direction. A second source of error is in the assumption that the refractive index remains constant downstream of the shock. As the bow shock curves from its tip region, the fluid properties and, therefore, the refractive index changes. However, the success of the numerical calculation in capturing all

features of the light scattering phenomena indicate that the above concerns are of secondary importance.

## V. CONCLUSION

The physical appearance of the light scattering effects in the two optical situations considered in this paper is very different. In the shadowgraph situation a wide central dark band and a few fringes are observed, while in a narrow laser beam and shock interaction situation long streaks in the farfield are observed. However, a closer look reveals many similarities. First, splitting of the main laser beam in the latter can be attributed to the shock shadow formation similar to that seen in the shadowgraph situation. Second, both situations involve light propagating tangential to the shock surface. The bow shock, considered in the present work, is a 3-D surface of revolution. In the shadowgraph image of Fig. 2, light has passed through every part of this surface; however, the shock shadow appears as a single line along the outer edge of the surface. Noticeably, only along this line, light rays are at a grazing incidence on the shock surface— identical to the situation when long light streaks are found to appear from a narrow laser beam. Third, upstream fringes and the upstream part of the light streaks are weaker than their downstream counterparts.

Perhaps, a physical explanation unifying the two optical situations can be best provided from the Geometrical Theory of Diffraction.[16,17,9] According to this theory, electromagnetic diffraction of high frequency waves by straight edges gives rise to cylindrical diffraction edge waves. The total diffracted field, observed on the screen, is a sum of the incident waves and the edge waves. In a shadowgraph situation the spatial extent of the incident field is very large and the edge waves interfere with this field to produce the fringe patterns seen upstream and downstream of the shock. On the other hand, the use of a laser beam of narrow spatial extent separates away the edge waves which then appear as the diverging light sheet from the point of its generation. A good example is the numerically calculated scattered light pattern shown in Fig. 12(b). The intensity distribution shows fringe formation only in the paraxial region where light from the undisturbed beam also appears.

The effect of the refractive index jump, caused by a change in the free stream Mach number and total pressure, on the light scattering phenomena are studied in the present paper. Use of a different wavelength of light is also expected to change the scattering pattern, as in any other situation involving diffraction. A fourth parameter of interest is the thickness of the shock, which is estimated to be of the order of light wavelength[3] (light wavelength: 633 nm; shock thickness for the experimental range: 150–750 nm). Direct measurement of the shock thickness was not possible in the present experiment. Inclusion of this parameter in the numerical modeling requires complete solution of the Helmholtz equation. Moreover, the experimental observation, that the light scattering phenomena are independent of the polarization of the incident field, indicates that the high-frequency approximation is valid for this situation. The shock, therefore, is assumed to be of zero thickness for all analysis.

## ACKNOWLEDGMENT

[1]W. Merzkirch, *Flow Visualization* (Academic, New York, 1987).

[2]M. Born and E. Wolf, *Principles of Optics*, Sixth ed. (Pergamon, New York, 1989).

[3]J. Panda, "Partial spreading of a laser beam into a light sheet by shock waves and its use as a shock detection technique," NASA CR-195329, 1994.

[4]J. Panda, "Wide angle light scattering in shock–laser interaction," to be published in AIAA J. (1995).

[5]J. Panda, "Shock detection technique based on light scattering by shock," to be published in AIAA J. (1995).

[6]J. A. Waltham, P. F. Cunningham, R. N. Michaelis, R. N. Campbell, and M. Notcutt, "The application of the refractive fringe diagnostic to shocks in air," Opt. Laser Technol. **19**, 203 (1987).

[7]L. A. Vasil'ev, *Schlieren Methods* (Israel Program For Scientific Translations, Israel, 1971).

[8]H. J. Pfeifer, H. D. Vom Stein, and B. Koch, "Mathematical and experimental analysis of light diffraction on plane shock waves," Proc. Int. Cong. High-Speed Photogr. **9th**, 423 (1970).

[9]P. Langois, R. A. Lessard, and A. Boivin, "Real-time curvature radii measurements using diffraction edge waves," Appl. Opt. **24**, 1107 (1985).

[10]D. O. Davis, W. R. Hingst, and J. Bodner, "Flow coefficient behavior for isolated normal and 20 degree boundary-layer bleed holes," NASA TM-106816, 1994.

[11]L. Z. Kriksunov and A. E. Pliev, "Refraction of laser beams at a compression shock," Sov. J. Opt. Technol. **51**, (1984) (English translation by The Optical Society of America, 1985), pp. 375–377.

[12]D. F. Hornig, "Shock front measurements by light reflectivity," in *Physical Measurements in Gas Dynamics and Combustion*, edited by R. W. Ladenburg (Princeton University Press, Princeton, NJ, 1954), pp. 203–210.

[13]W. L. Lewis, R. E. Teets, J. A. Sell, and T. A. Seder, "Temperature measurements in a laser-heated gas by quantitative shadowgraphy," Appl. Opt. **26**, 3695 (1987).

[14]H. J. Weaver, *Applications of Discrete and Continuous Fourier Analysis* (Wiley, New York, 1983).

[15]W. H. Press, B. P. Flannery, S. A. Tuekolsky, and W. T. Vetterling, *Numerical Recipes, The Art of Scientific Computing* (Cambridge University Press, Cambridge, 1986).

[16]J. B. Keller, "Geometrical theory of diffraction," J. Opt. Soc. Am. **52**, 116 (1962).

[17]R. G. Kouyoumjian, "The geometrical theory of diffraction and its application," in *Numerical and Asymptotic Techniques in Electromagnetics*, edited by R. Mittra (Springer, New York, 1975), pp. 165–215.